U. S. Army Ordnance
Ballistics Research Laboratory
Aberdeen Proving Ground, Maryland
Approved Proposal No. 3175
Authorization No. 4086

EXPLOSIVES RESEARCH LABORATORY

HYPERVELOCITY IMPACT PHENOMENA

Quarterly Report
June 1, 1962 to August 31, 1962

BUREAU OF MINES, PITTSBURGH, PA.

UNITED STATES
DEPARTMENT OF
THE INTERIOR

HYPERVELOCITY IMPACT PHENOMENA

Quarterly Report

June 1, 1962 to August 31, 1962

Prepared for:

U. S. Army Ordnance
Ballistic Research Laboratory
Aberdeen Proving Ground, Maryland
Approved Proposal No. 3175
Authorization No. 4086

by

Karl R. Becker

Richard W. Watson

Frank C. Gibson

Approved by:

Robert W. Van Dolah, Chief
Explosives Research Laboratory

U. S. Department of the Interior
Bureau of Mines
Pittsburgh, Pa.
November 9, 1962

HYPERVELOCITY IMPACT PHENOMENA

Introduction

A considerable amount of data have been accumulated and analyzed describing the character of spall fragments resulting from the impact on thin targets by high velocity projectiles. In these tests the projectile velocity has been varied while the projectile material and its geometry (hence its mass) have been kept constant. The projectiles used were steel cylinders with both the diameter and length equal to 1/16 inches having a mass of about 24 mg.; these are designated as Scale I, steel projectiles.

Some data are now available for Scale II, steel projectiles, i.e., the linear dimensions of the projectile are scaled by a factor of two and the mass by a factor of eight; the Scale II projectiles are steel cylinders having a diameter and length of 1/8 inches and a mass of about 190 mg. The Scale II explosive projector is shown in figure 1 and provides the same projectile velocity as one of the Scale I projector systems (3.2 km/sec.).

The scope of work accomplished with Scale II projectors involves studies on three thicknesses of aluminum, 2024-T3, targets; the population distribution and mass distribution of spall particles have been determined and compared with similar results from Scale I impacts. Futhermore, the availabilities of Scale II data allows scaling between Scale I and Scale II impact by comparison of total numbers and masses of spall particles.

Behind-Target Effects

Spall Population Distribution Data (Scale II Projectiles)

Population distribution data were derived from Scale II projectiles impacting three thicknesses (3/16, 1/4, and 3/8 inches) of aluminum (2024-T3) targets at normal incidence. The spall material penetrated a thin aluminum witness foil located 6.5 inches beneath the target plate. The physical set-up of projector, target plate, and witness foil as well as treatment of data is identical to that described in earlier reports for Scale I projectiles[1/]. The basic data are tabulated in table I which gives the number of spall fragments found in each element of solid angle for each target thickness group. The reduced data are plotted and compared with former Scale I data in figure 2. The plot gives $\frac{1}{N}\frac{\Delta N}{\Delta \Omega}$ vs $\frac{\theta}{2}$ and may be thought of as depicting the percentage of the total population density plotted against the angle $\frac{\theta}{2}$ which is a measure of the radial distance out from the center of spall impact. The solid curve shown, represents the data from similar Scale I results; the Scale II data points fit the curve quite well and one may reasonably conclude that the percentage of the total number of fragments found in any given element of solid angle is independent of the projectile scale size. Also, the fragments having higher penetration capabilities are not distributed differently than

---

1/ Becker, K. R., Watson, R. W., and Gibson, F. C., Hypervelocity Impact Phenomena: Bureau of Mines, November 1961 (Preliminary Background Report).

are fragments for the whole aggregate group. The solid circles on the plot represent the 20% group with somewhat higher penetration capabilities and these data points are essentially the same as those representing the aggregate group. The distribution for the 20% group was obtained by filtering out 80% of the particles with additional thicknesses of witness foil and taking a distribution for those particles capable of penetrating the additional foil. Data for the 20% group are tabulated in table II.

Spall Mass Distribution Data (Scale II Projectiles)

Mass distribution data for Scale II projectiles impacting three thicknesses of aluminum (2024-T3) targets at normal incidence were obtained by gelatin collection methods described in earlier reports. The gelatin collection method involves an actual recovery of spall material found in various ring elements and allows a chemical separation of projectile particles from target particles. The distributed target and projectile particle masses are given in tables III and IV respectively. The data from table III, (target spall masses) are reduced by $\frac{1}{M}$, averaged over target thicknesses, and plotted against $\frac{\theta}{2}$ on figure 3. The solid curve shown is for the previously tested Scale I projectiles and the plot shows that there is a reasonable fit between the Scale II data points and the Scale I curve. The significance of the plot is that the percentage of the total target spall mass found in a given element of solid angle behind the target is

independent of the projectile scale size.

The distributed projectile masses are not plotted but the data are included in table IV for possible use in subsequent analyses of spall phenomena. However, the total recovered projectile masses, also found in table IV, are of some immediate interest insofar as scaling relationships between Scale I and Scale II are concerned. This is discussed in the following section. For the moment, it will suffice to say that about 70% to 90% of the original Scale II projectile mass is recovered behind the target; this is in general agreement with results from Scale I projectiles.

Scaling Relationships

The term "scaling", as used here, refers to the manner in which the total number of spall particles and total mass of spall particles increases when the projectile dimensions are scaled upward while the projectile velocity is kept constant. The total numbers and masses of spall particles produced by impacting various thicknesses of 2024-T3 aluminum targets with Scale I projectiles are compared, with similar results, with Scale II projectiles impacting scaled target thicknesses. Comparisons and scaling relations for both projectile particles and target particles have been separately determined.

The total masses and numbers as a function of target thickness for both Scale I and Scale II impacts are given in tables V and VI. The upper portion of the tables gives absolute numbers and masses

while the lower portion of the tables contain reduced numbers and masses. Reduction of numbers and masses, is accomplished by dividing by appropriate powers of the scale factor, the powers having been chosen by consideration of peak shock pressures developed at the bottom surface of the target plates.

The first scaling relation is illustrated in figure 4 and deals with the numbers of target spall particles. The plot gives $\frac{N}{f^2}$ vs $\frac{t}{f}$ where N = number of spall particles, t = target thickness, and f is the scale factor. Plotting the data in this manner appears to bring the Scale I and Scale II data points in reasonable coincidence at given reduced target thickness. The plot shows that if one scales the dimensions of the projectile and the target thickness by a factor of two, then one can expect the number of target spall fragments to increase by a factor of four. A possible explanation for this behavior is that the number of particles per unit area of spall surface is determined by the peak pressure at the second surface (bottom interface of the target) and in order to realize identical peak pressures the targets for Scale II impacts must be scaled.

The second scaling relationship is illustrated in figure 5 and deals with the total mass of target spall. The plot shows $\frac{M}{f^3}$ vs $\frac{t}{f}$ and is interpreted to mean that when the projectile dimensions and target thickness are increased by a factor of two, one can expect eight times the target spall mass from impacts with Scale II projectiles as opposed to impacts with Scale I projectiles. Thus, since

the Scale II impacts produce four times the number of spall particles having eight times as much mass than the average mass per particle is twice that developed by impacts with Scale I projectiles.

Similar comparisons for the numbers and masses of projectile particles recovered after penetrating the targets are given in figures 6 and 7. Figure 6 shows that the factor $\frac{1}{f^3}$ applied to N brings the Scale I and Scale II data points into reasonable coincidence while in figure 7 the factor $\frac{1}{f^3}$ applied to M does the same. Thus, the two plots taken together show that, at a given reduced target thickness, the Scale I and Scale II projectiles break up in a somewhat similar manner i.e., the average particle size is approximately the same. One obtains eight times the number and mass from Scale II projectiles simply because the volume of a Scale II projectile is larger by a factor of eight. One other significant feature of the data shown in figure 7 is that the total recovered projectile mass is essentially independent of target thickness.

Summary of Behind-Target Effects

Within the limits of scale sizes tested, the qualitative features of the population distribution and of the distribution of spall mass are not altered when the projectile is scaled; the percentage of the total number or total mass of spall particles found in a given element of space behind the target is independent of the projectile scale size.

(2) In a given spall system, the spall particles having higher penetration capabilities do not appear to be distributed differently than the aggregate group.

(3) Scaling of the projectile appears to affect the spall systems from scaled targets in the following manner:

(a) The number of target spall particles is proportional to the square of the projectile scale size.

(b) The number of projectile particles is proportional to the cube of the scale size.

(c) The mass of both the target spall and projectile particles is proportional to the cube of the projectile scale size.

Table I. Tabulation of data relative to the population distribution of spall particles behind various thicknesses of aluminum 2024-T3 targets; the targets were impacted by Scale II, 3.2 km/sec projectiles at normal incidence.

Ring	(Sterad.)	θ/2 (deg)	Average Number of Fragments (Δ N) Target Thickness (in.) (3/16)	(1/4)	(3/8)
1	.018	4.4	82 (4550)	45 (2500)	132 (7330)
2	.056	8.7	214 (3820)	166 (2960)	224 (4000)
3	.087	13.0	237 (2720)	257 (2950)	143 (1640)
4	.117	17.1	277 (2370)	290 (2480)	88 (752)
5	.141	21.1	284 (2010)	241 (1710)	32 (227)
6	.160	24.8	328 (2050)	134 (837)	17 (106)
7	.173	28.3	256 (1480)	89 (514)	12 (69)
8	.181	31.6	145 (801)	63 (348)	10 (55)
9	.185	34.7	74 (400)	31 (168)	6 (32)
10	.186	37.6	46 (249)	23 (124)	9 (49)
11	.184	40.2	20 (108)	12 (65)	3 (16)
12	.179	42.7	13 (73)	15 (84)	5 (28)
	Total		2004	1407	695

Notes: (1) The populations given here include both projectile material and target material.

(2) Numbers in parentheses are $\Delta N/\Delta \Omega$ and represent population density.

(3) θ/2, is specified at the midpoint of the interval.

Table II. Tabulation of data relative to the population distribution of spall particles behind various thicknesses of 2024-T3 aluminum targets; the targets were impacted by Scale II, 3.2 km/sec projectiles at normal incidence. The populations given here include only the 20% from Table I having the highest penetration capability.

Ring	$\Delta\Omega$ (Sterad.)	$\theta/2$ (deg)	Average Number of Fragments (ΔN) Target Thickness (in.) (3/16)	(1/4)	(3/8)
1	.018	4.4	25 (1390)	14 (780)	18 (1000)
2	.056	8.7	61 (1090)	38 (680)	21 (375)
3	.087	13.0	79 (908)	51 (586)	14 (161)
4	.117	17.1	73 (624)	59 (504)	11 (94)
5	.141	21.1	75 (532)	46 (326)	7 (50)
6	.160	24.8	62 (387)	21 (131)	3 (19)
7	.173	28.3	40 (231)	15 (87)	4 (23)
8	.181	31.6	19 (105)	14 (77)	3 (16)
9	.185	34.7	14 (76)	7 (38)	3 (16)
10	.186	37.6	8 (43)	5 (27)	4 (22)
11	.184	40.2	5 (27)	3 (16)	2 (11)
12	.179	42.7	2 (11)	4 (22)	1 (6)
	Total		478	290	95

Notes: (1) Numbers in parentheses are $\Delta N/\Delta\Omega$ and represent population density.

(2) $\theta/2$, is specified at the midpoint of the interval.

Table III. Tabulation of data associated with the distribution of target spall masses found in the spall behind thin aluminum 2024-T3 targets which were impacted by Scale II, 3.2 km/sec projectiles at normal incidence.

Solid Angle Interval ($\Delta\Omega$)	Displacement Angle (deg) ($\theta/2$)	Average Mass of Target Spall Particles (mg) $\pm\sigma$ — Target Thickness (in.) (3/16) ΔM	σ	(1/4) ΔM	σ	(3/8) ΔM	σ
.074	4.4	68 (917)	34	85 (1148)	39	262 (3541)	252
.204	13.0	92 (452)	24	137 (672)	27	226 (1108)	204
.300	21.1	61 (203)	35	157 (523)	41	330 (1100)	341
.354	28.3	87 (241)	20	80 (226)	20	143 (404)	42
.371	34.7	70 (189)	31	67 (179)	26	85 (229)	66
.363	40.2	31 (85)	7	33 (90)	6	85 (234)	93
	Total Average Mass (mg)	410	89	559	144	1132	681

Notes: (1) Masses given here, include target material only (projectile particles are excluded).

(2) Numbers in parentheses are $\Delta M/\Delta\Omega$.

(3) σ = range/$\sqrt{n}$ ($n = 3$).

(4) Displacement angle is specified at the midpoint of the interval.

Table IV. Tabulation of data associated with the distribution of projectile particle masses in the space behind thin aluminum 2024-T3 targets impacted by Scale II, 3.2 km/sec projectiles at normal incidence.

Solid Angle Interval ($\Delta\Omega$)	Displacement Angle (deg) ($\theta/2$)	Average Mass of Projectile Fragments (mg) $\pm\sigma$ — Target Thickness (in.) (3/16) ΔM	σ	(1/4) ΔM	σ	(3/8) ΔM	σ
.074	4.4	25 (344)	8	59 (796)	21	81 (1095)	31
.204	13.0	35 (170)	5	54 (265)	13	53 (260)	23
.300	21.1	24 (81)	6	21 (71)	5	17 (57)	14
.354	28.3	18 (50)	13	3 (7)	1	7 (20)	3
.371	34.7	16 (42)	17	3 (9)	2	4 (11)	4
.363	40.2	12 (32)	7	2 (6)	2	6 (17)	3
	Total Average Mass (mg)	130	6	142	14	167	9

Notes: (1) Masses given here include only projectile material coming through the target.

(2) Numbers in parentheses are $\Delta M/\Delta\Omega$.

(3) σ = range/ $\sqrt{n}$ (n = 3).

(4) Displacement angle is specified at the midpoint of the interval.

Table V. Tabulation of data associated with Figure 3 and Figure 4. The data pertains to the scaling of the total numbers and masses of target spall particles obtained from impacting aluminum 2024-T3 targets with both Scale I and Scale II, steel projectiles at normal incidence.

	Scale I Data			Scale II Data		
t(in.)	3/32	1/8	3/16	3/16	1/4	3/8
t/f(in.)	3/32	1/8	3/16	3/32	1/8	3/16
N(#)	818	300	126	2,462	1,300	611
M(mg)	34	66	80	410	559	1,132
N/f^2(#)	818	300	126	615	325	152
M/f^3(mg)	34	66	80	51	70	141

Notes: t = Target thickness.

N = Number of target spall particles.

M = Mass of target spall particles.

f = Scale factor.

Table VI. Tabulation of data associated with Figure 5 and Figure 6. The data pertains to the scaling of the total numbers and masses of projectile particles resulting from Scale I and Scale II projectiles penetrating aluminum 2024-T3 targets at normal incidence.

	Scale I Data			Scale II Data		
t(in.)	3/32	1/8	3/16	3/16	1/4	3/8
t/f(in.)	3/32	1/8	3/16	3/32	1/8	3/16
N(#)	111	184	89	1930	1500	551
M(mg)	24	23	21	130	142	167
N/f^3(#)	111	184	89	241	187	69
M/f^3(mg)	24	23	21	16	18	21

Notes: t = Target thickness.

N = Number of projectile particles.

M = Mass of projectile particles.

f = Scale factor.

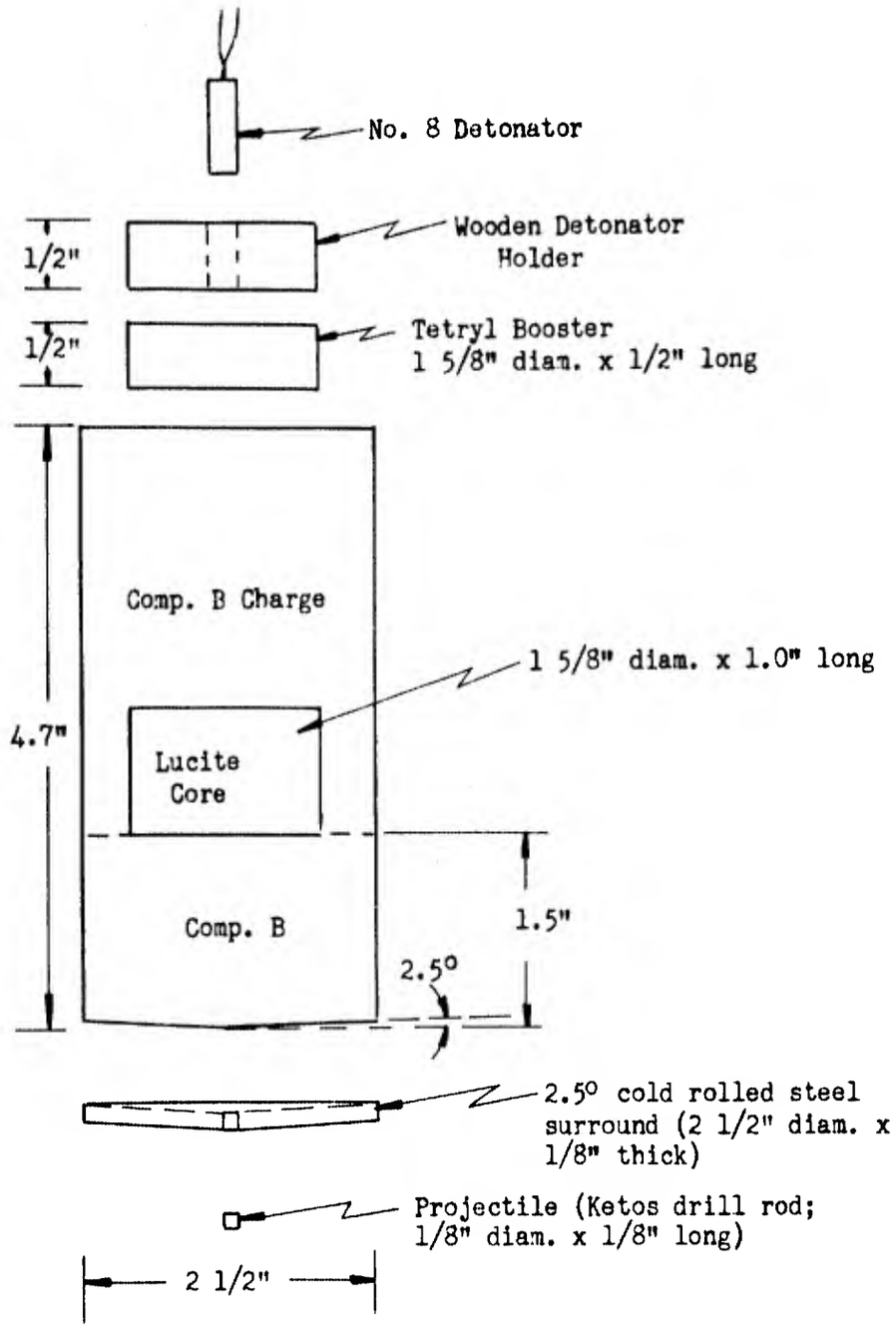

Fig. 1 Sketch of an explosive projector that propels a Scale II, steel projectile at a velocity of 3.2 km/sec.

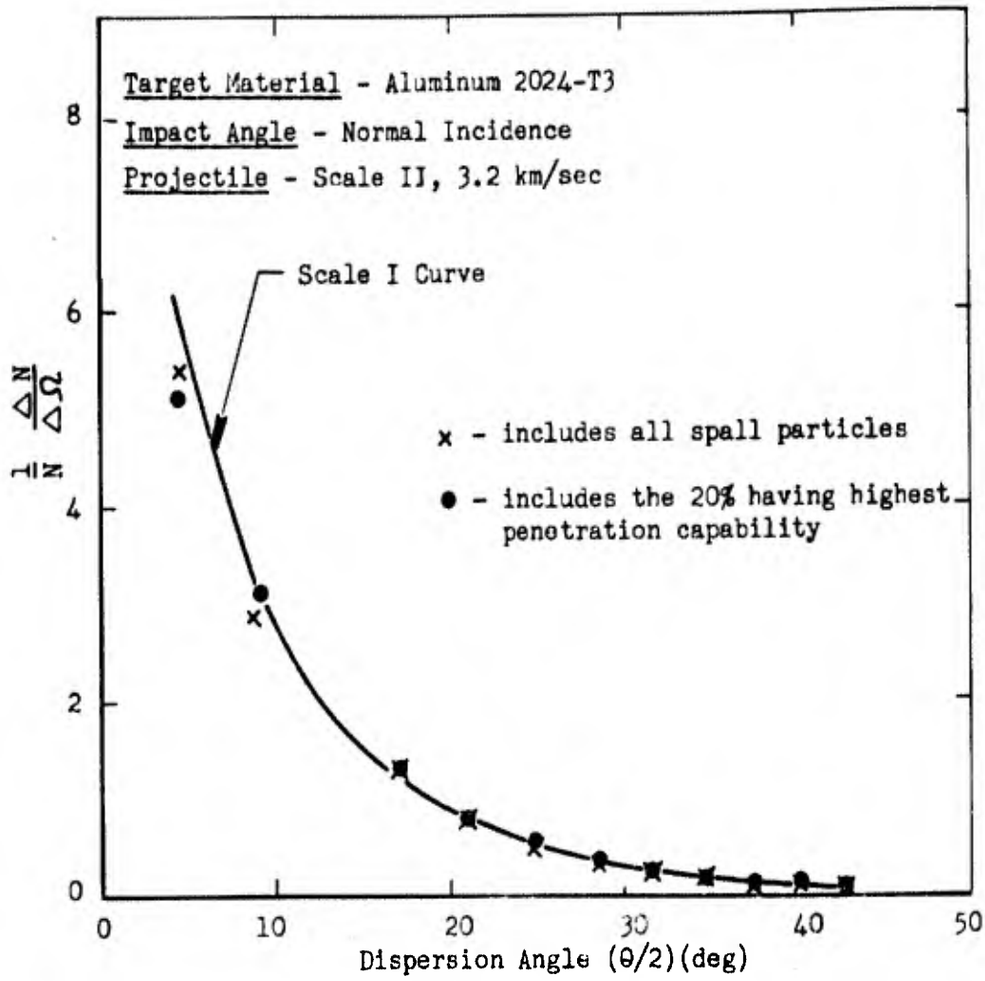

Fig. 2 Normalized spall population distribution data for Scale II, 3.2 km/sec projectiles compared with similar data for Scale I projectiles.

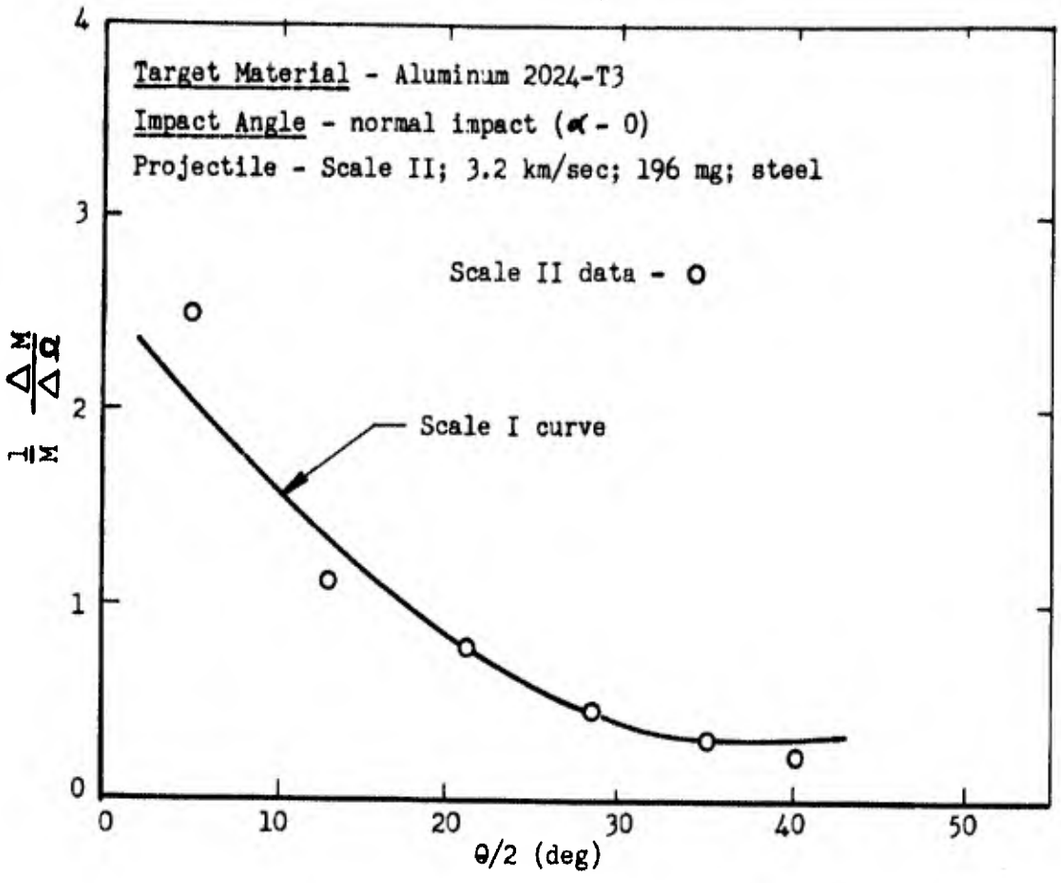

Fig. 3 Normalized target spall, mass distribution data for Scale II 3.2 km/sec projectiles compared with similar results for Scale I projectiles. The data have been averaged over the target thickness.

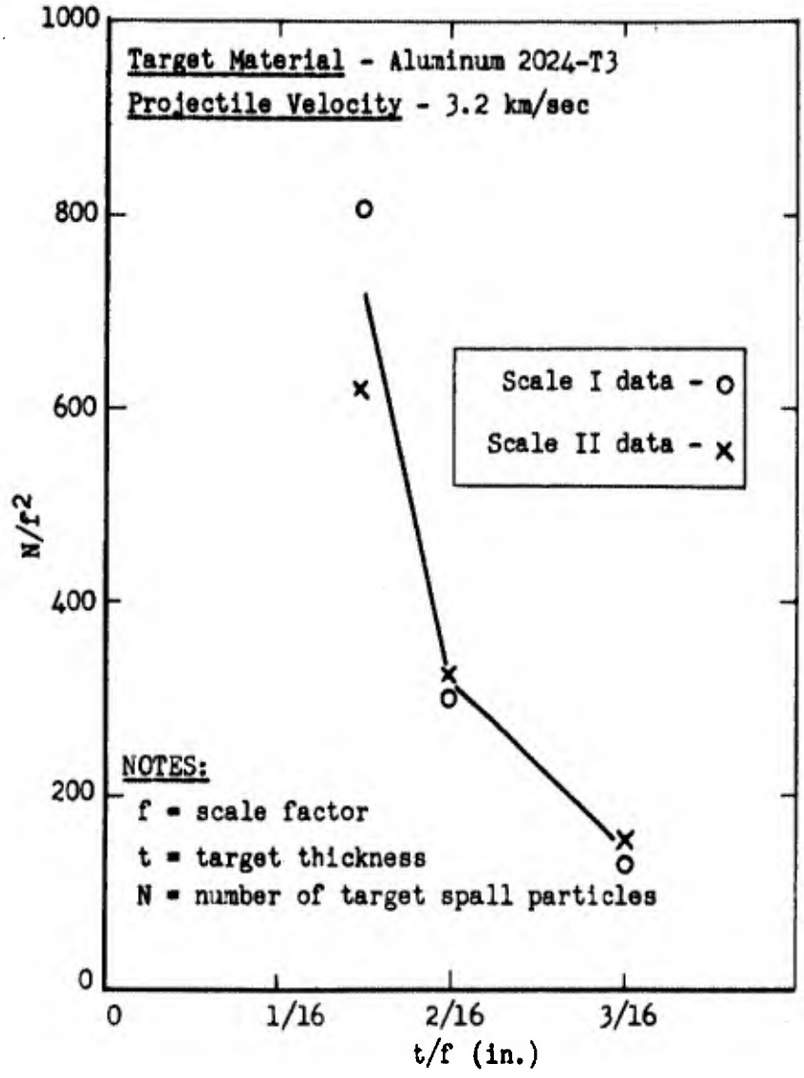

Fig. 4 Plot illustrating an interpretation of the scaling effect for the number of target spall particles produced by projectiles impacting thin targets.

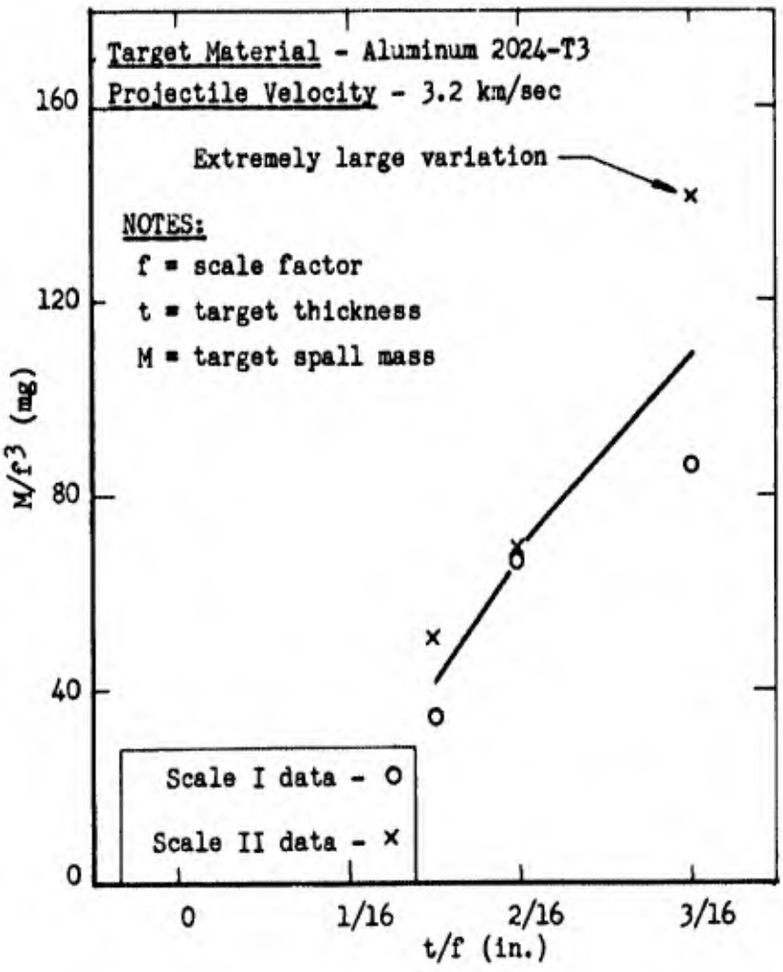

Fig. 5 Plot illustrating an interpretation of a scaling effect for target spall mass produced by projectiles impacting thin aluminum alloy targets.

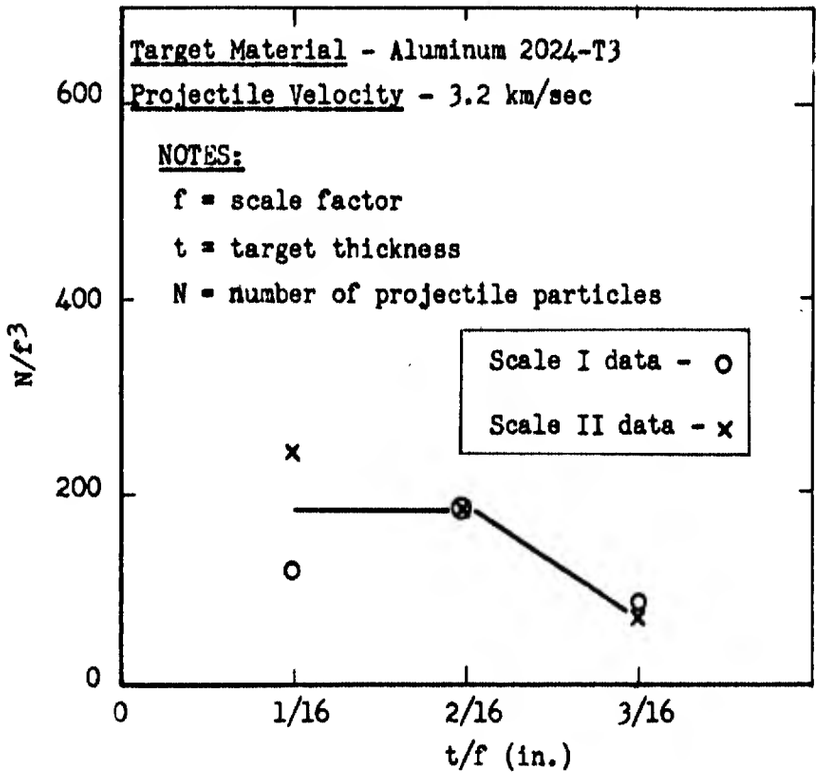

Fig. 6 Plot illustrating an interpretation of a scaling effect for the number of projectile particles produced due to projectile breaking up after having penetrated thin targets.

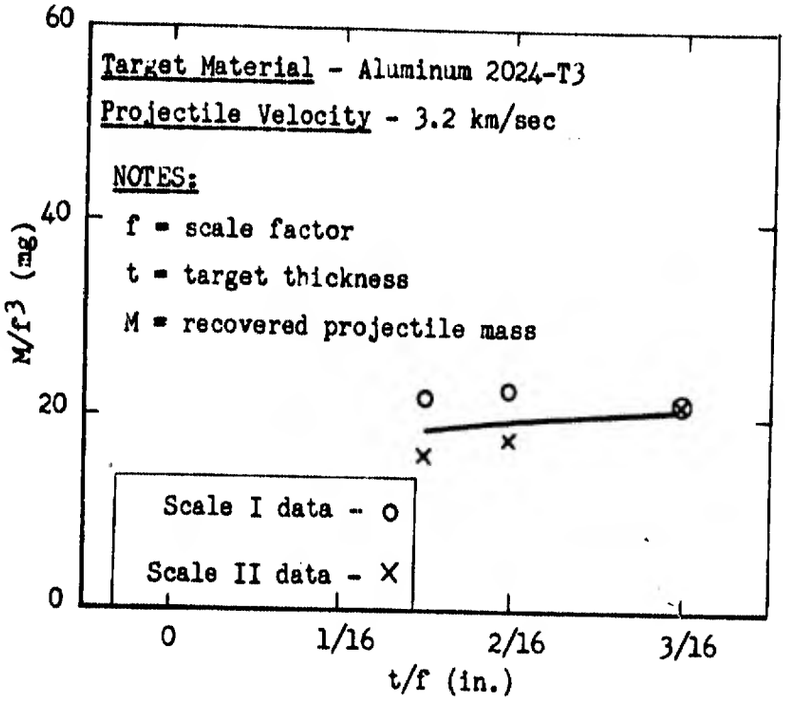

Fig. 7 Plot illustrating the scaling effect for recovered projectile mass resulting from scaled projectiles penetrating aluminum alloy targets.

DISTRIBUTION LIST FOR

Type I Quarterly Report

on

Hypervelocity Impact Phenomena

Sponsored by the Department of the Army
Aberdeen Proving Ground

Commanding General
Aberdeen Proving Ground
Maryland
Attn: R. J. Eichelberger
Ballistic Research Laboratories

Commanding General
Aberdeen Proving Ground
Maryland
Attn: J. Kineke
Ballistic Research Laboratories

Commanding General
Aberdeen Proving Ground
Maryland
Attn: Technical Library
Ballistic Research Laboratories

Office, Chief of Ordnance
Department of the Army
Washington 25, D. C.
Attn: ORDTU

British Joint Services Mission
1800 K Street, N. W.
Washington 6, D. C.
Attn: Reports Officer

Commanding Officer
U. S. Naval Ordnance Test Station
China Lake, California
Attn: J. W. Rogers

Commanding Officer
Air Proving Ground Center
Eglin Air Force Base, Florida
Attn: H. L. Davis

Commanding General
Aberdeen Proving Ground
Maryland
Attn: S. Kronman
Ballistic Research
Laboratories

Commanding General
Aberdeen Proving Ground
Maryland
Attn: F. E. Allison
Ballistic Research
Laboratories

Office, Chief of Ordnance
Department of the Army
Washington 25, D. C.
Attn: ORDTB, Ballistics Section
Mr. M. C. Miller

Commanding Officer
Armed Services Technical Information Agency
Arlington Hall Station
Arlington 12, Virginia
Attn: TIPCR

Canadian Army Staff
2450 Massachusetts Avenue
Washington 8, D. C.

Director
U. S. Naval Research Laboratory
Washington 25, D. C.
Attn: Mr. W. W. Atkins, Code 130

Commanding Officer
Air Proving Ground Center
Eglin Air Force Base, Florida
Attn: Lt. W. H. Dittrich
Det. 4, ASD(ASQWR)

Director, The RAND Corporation
1700 Main Street
Santa Monica, California
Attn: J. H. Huth

Director, The RAND Corporation
1700 Main Street
Santa Monica, California
Attn: R. L. Bjork

Director, The RAND Corporation
1700 Main Street
Santa Monica, California
Attn: Technical Library

Library of Congress
Technical Information Division
Reference Department
Washington 25, D. C.
Attn: Bibliograph Section

General Motors Corporation
Defense Systems Div., Box T
Santa Barbara, California
Attn: J. W. Gehring

Firestone Tire & Rubber Company
1200 Firestone Parkway
Akron, Ohio
Attn: C. M. Cox

Commanding Officer
Air Proving Ground Center
Eglin Air Force Base, Florida
Attn: F. E. Howard
Det. 4, ASD(ASQP)

Director, National Aeronautics & Space Administration
Ames Research Center
Moffett Field, California
Attn: J. L. Summers

Director, National Aeronautics & Space Administration
Ames Research Center
Moffett Field, California
Attn: Technical Library

Director, National Aeronautics & Space Administration
Langley Research Center
Langley Field, Virginia
Attn: W. H. Kinard

Director, National Aeronautics & Space Administration
Langley Research Center
Langley Field, Virginia
Attn: Technical Library

General Motors Corporation
Defense Systems Div., Box T
Santa Barbara, California
Attn: Technical Library

Aeroelastic & Structures Laboratory
Massachusetts Institute of Technology
77 Massachusetts Avenue
Cambridge 39, Massachusetts
Attn: W. Herrmann

Drexel Institute of Technology
Mechanical Engineering Dept.
Philadelphia 4, Pennsylvania
Attn: Pei Chi Chou

National Aeronautics and Space Administration
Lewis Research Center
21000 Brookpark Road
Cleveland 35, Ohio

UNCLASSIFIED